ACS OMEGA

http://pubs.acs.org/journal/acsodf

Article

Purely Organic Microparticles Showing Ultralong Room Temperature Phosphorescence

Heidi Thomas, Felix Fries, Max Gmelch, Toni Bärschneider, Martin Kroll, Thaleia Vavaleskou, and Sebastian Reineke*

Cite This: *ACS Omega* 2021, 6, 13087−13093

Read Online

ACCESS | Metrics & More | Article Recommendations | Supporting Information

ABSTRACT: Currently, organic phosphorescent particles are heavily used in sensing and imaging. Up to now, most of these particles contain poisonous and/or expensive metal complexes. Environmentally friendly systems are therefore highly desired. A purely amorphous system consisting of poly(methyl methacrylate) particles with incorporated *N,N,N′,N′*-tetrakis(4-carboxyphenyl)-benzidine emitter molecules is presented in this work. Single particles with sizes between 400 and 840 nm show—depending on the environment—bright fluorescence and phosphorescence. The latter is observed when oxygen is not in the proximity of the emitting dye molecules. These particles can scavenge singlet oxygen, which is produced during the photoexcitation process, by incorporating it into the polymer matrix. This renders their use to be unharmful for the surrounding matter with possible application in marking schemes for living bodies.

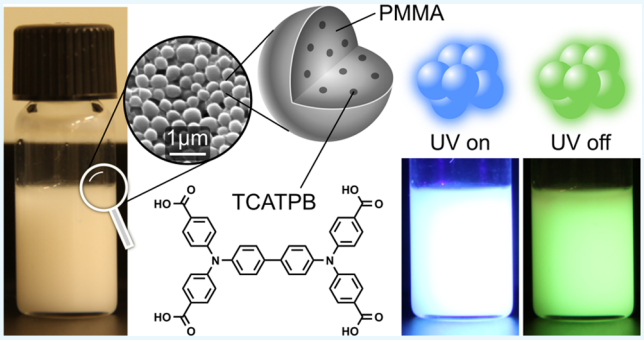

INTRODUCTION

In the last years, small organic phosphorescent particles have been successfully used in a variety of devices for sensing and imaging.[1] They can be incorporated in chemical sensors[2−5] or light-emitting diodes,[6−8] used in O_2 sensing,[9,10] for in vivo imaging,[11] or in phosphorescent immunoassays.[12,13] Most of the organic particles discussed in the literature contain metal complexes such as Pt(II),[14−16] Ir(III),[17−19] Eu(III),[20] or others.[21,22] Since the heavy metal effect induces an efficient spin−orbit coupling, they have long been used to promote organic phosphorescence.[23,24] The aim for environmentally friendly alternatives, low cost, and easy processability led to a huge effort in the preparation of small purely organic particles showing room temperature phosphorescence (RTP). Several strategies can be pursued, including H-Aggregates,[25−28] encapsulation,[29,30] polymerization,[31,32] and host-guest doping.[33,34] The big advantage of RTP concerning in vivo imaging is the enhanced signal-to-noise ratio compared to fluorescence since in the afterglow emission, no luminescent background signal is present.[25] However, many metal-free organic room temperature materials are nano- or microcrystals. In contrast to this, purely amorphous systems are easy to process and hence attract a lot of scientific interest.

Here, we present poly(methyl methacrylate) (PMMA) particles with incorporated *N,N,N′,N′*-tetrakis (4-carboxyphenyl)benzidine (TCATPB) emitter molecules. It has already been shown that this material combination shows bright phosphorescence in thin films and three-dimensional (3D) printed objects.[35] Downscaling such a fundamentally simple and flexible system to particles smaller than 1 μm adds to the wide application areas mentioned above. These particles do not contain any harmful heavy elements and have the advantage over the already mentioned techniques that they do not require high temperatures, expensive educts, or complex workup. Depending on the oxygen content of the environment, the fluorescence and phosphorescence of single particles can be observed in a luminescence microscopy setup.

RESULTS AND DISCUSSION

Preparation of the Particles. PMMA:TCATPB particles were formed using the so-called emulsion polymerization,[36] a type of radical polymerization. Methyl methacrylate (MMA), ethylene glycol dimethacrylate (EGDMA, linker), and the emitter were emulsified in water containing sodium dodecyl sulfate (SDS, surfactant) and potassium persulfate ($K_2S_2O_8$, initiator) by vigorous stirring. Upon heating the solution, the particles were formed. The polymer particles were separated by centrifugation and washed three times with water to remove unbound monomers and residues such as of the initiator. The

Received: February 11, 2021
Accepted: April 9, 2021
Published: May 10, 2021

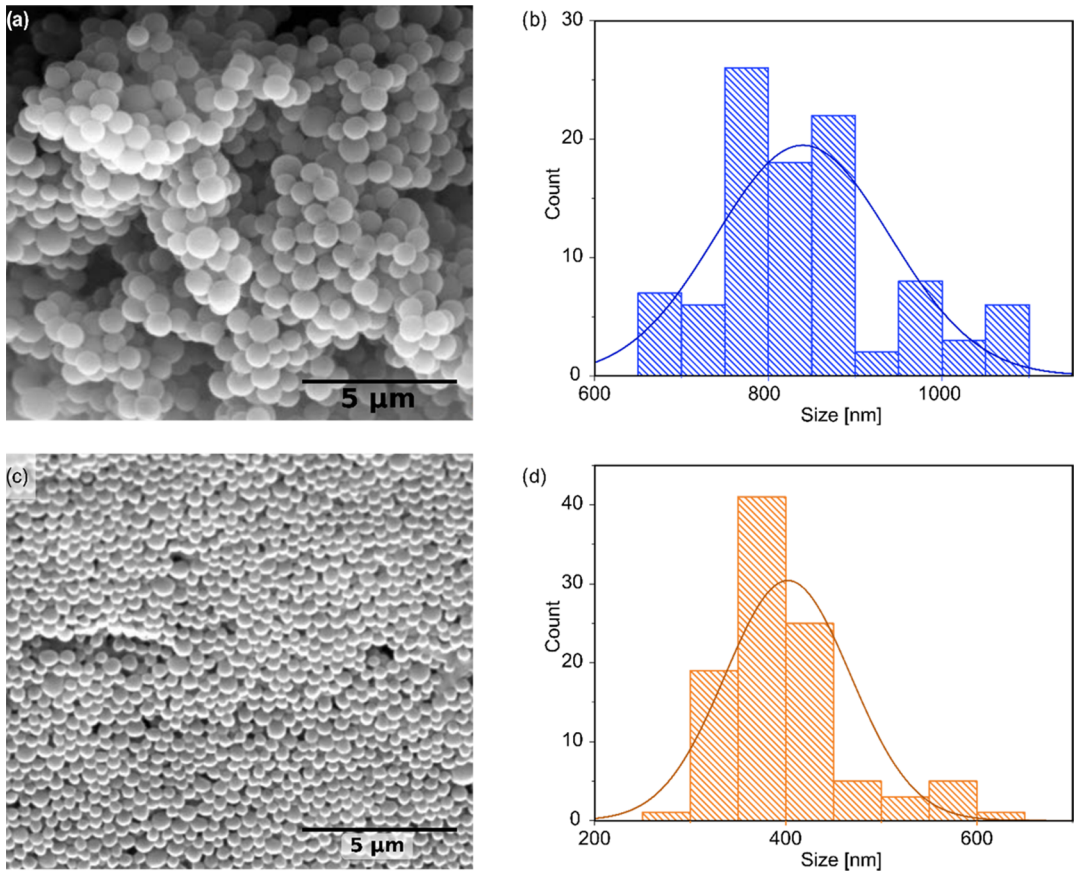

Figure 1. SEM images (a, c) as well as size-distribution diagrams (b, d) of the larger P_{840} (blue) and smaller particles P_{400} (orange).

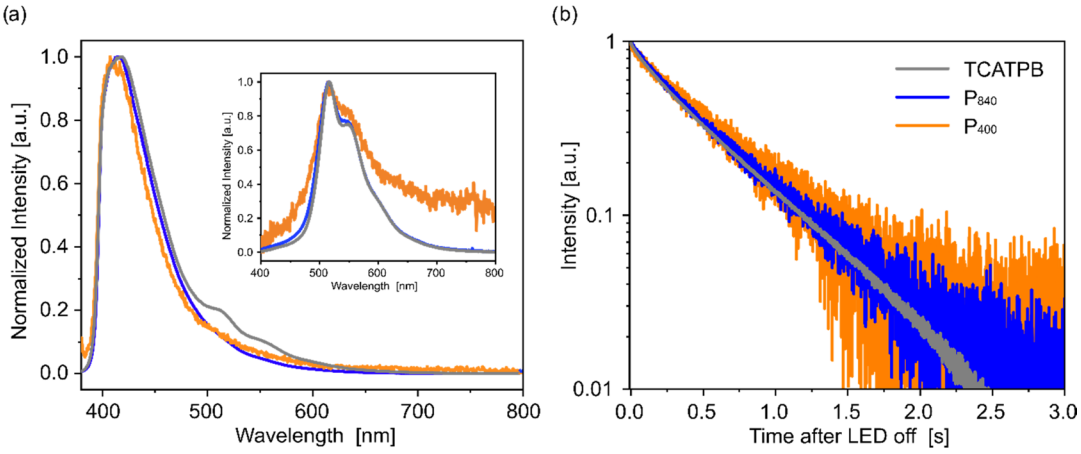

Figure 2. Thin-film emission data of TCATPB (gray) in PMMA covered with Exceval as well as P_{840} (blue) and P_{400} (orange) embedded in Exceval in the ambient atmosphere at an excitation wavelength of λ_{exc} = 365 nm. (a) Prompt emission showing both fluorescence and phosphorescence. The inset shows delayed spectra showing the phosphorescence only. (b) Corresponding phosphorescence decays with τ_{Phos} = 575 ms (TCATPB), 585 ms (P_{840}), and 610 ms (P_{400}).

particles were redispersed and stored in water to prevent clogging. TCATPB was dissolved in cyclohexanol since it is not soluble in MMA and/or EGDMA. The advantage of cyclohexanol is that it does not dissolve the formed particles. Particles with two different sizes were prepared. For the formation of the smaller ones, no linker was used. The reason is that even though the increase of the SDS concentration led to smaller particle sizes, as was expected, the particles lacked phosphorescence. Polymerization using only the monomer instead gave smaller particles that showed RTP. This may be due to the better incorporation of the emitter into the PMMA particle.

Physical and Photophysical Properties of the Particles. Figure 1 shows scanning electron microscopy (SEM) images as well as size-distribution diagrams of the respective particles having mean sizes of around 840 nm (P_{840}) and 400 nm (P_{400}).

To measure the luminescent properties of the particles, they were applied onto a quartz substrate at a high concentration. This is achieved by embedding the particles into an oxygen

https://doi.org/10.1021/acsomega.1c00785
ACS Omega 2021, 6, 13087−13093

Table 1. Summary of the Emission (Fluorescence and Phosphorescence) of the Different Targets: PMMA:TCATPB, P_{840}, and P_{400} along with the Measured Fluorescence and Phosphorescence Lifetimes, Quantum Yield, and Radiative and Nonradiative Rates[a]

sample	λ_{fluo} [nm]	λ_{phos} [nm]	τ_{fluo} [ns]	τ_{phos} [ms]	k_{r_P} [s^{-1}][c]	k_{nr_P} [s^{-1}][c]	$\Phi_{fluo+phos}$ [%]
TCATPB	416	516/550	2.0	575/740[b]	1.35	0.39	36.2
P_{840}	416	516/548	1.8	585/760[b]	1.32	0.39	32.9
P_{400}	408	516/550	1.8	610/810[b]	1.23	0.40	33.2

[a]Thin film covered with and particles embedded in Exceval. All measurements performed under air at room temperature. [b]Measured at 77K. [c]See the Supporting Information for details.

barrier. The barrier (Exceval, a water-soluble ethylene vinyl alcohol polymer) does not emit itself and allows measurements in air. To detect the phosphorescence, the remaining oxygen within the particles has to be removed by activation with UV light. The activation over time by continuous excitation is shown in Figure S9 by the example of P_{840}. A detailed description of this process has been published recently.[37] As a reference system, a thin layer of TCATPB in PMMA on a quartz substrate was used. To ensure the same conditions as for the particles, the TCATPB sample has also been covered with a thin barrier layer. Figure 2 shows a comparison of the luminescent characteristics of P_{840}, P_{400}, and the reference system. The fluorescence maximum of P_{840} is located at 416 nm and does not differ from TCATPB (Figure 2a), whereas the maximum of P_{400} shows an 8 nm blue shift, which we attribute to random fluctuations. The phosphorescence ratio is weakened in the microparticle samples compared to the thin-film sample. It is assumed that the phosphorescence of a considerable amount of emitters in the microparticle samples is quenched with very high efficiency, leading to some of the emitters showing fluorescence only. Thus, the total phosphorescence ratio is reduced. Presumably, this is caused by the geometry of the two systems. In the microparticles, a significant amount of emitter molecules is embedded at the particles' surface, where they are prone to triplet-exciton quenching mediated through molecular oxygen present at this very surface. In contrast, the reference sample decouples all emitters from direct contact with oxygen.

Except for the signal-to-noise ratio, the phosphorescence of both kinds of particles resembles the spectrum of the reference (the inset of Figure 2a). All three samples show two peaks at around 516 and 550 nm. The triplet energy is therefore not impacted by the size of the system, which is in accordance with previous observations, suggesting that the triplet energy is mainly affected by modifications of the emitter molecules themselves.[38] The phosphorescence lifetime, on the other hand, potentially depends on the surrounding environment. Here, the lifetime slightly increases from 575 ms (TCATPB) to 585 ms (P_{840}) and 610 ms (P_{400}), with decreasing system size. A reason might be the missing linker in the case of P_{400} and therefore a slightly larger amount of methacrylate groups consequently exhibiting more hydroxy functions (by tautomerisation of methyl ester groups) per emitter molecule. As has already been reported,[34,39,40] hydrogen bonds formed between the emitter and the host lead to an enhancement of the phosphorescence. Nonetheless, the difference in the lifetime is not drastic, which is as expected, as each particle still contains plenty of emitter molecules (2.7×10^6 molecules per particle for P_{840} and 2.9×10^5 molecules per particle for P_{400}). Compared to other recently published organic phosphors,[41−43] this particle system compares well with a variety of organic molecules showing RTP, where a typical lifetime value range from a few hundred milliseconds up to single-digit seconds (Table 1).

Phosphorescence Imaging of the Particles. Using a fluorescence microscope, the particles were investigated with respect to their individual luminescence properties. Especially, the switching between purely fluorescent emission in air and additional phosphorescence in nitrogen needs to be confirmed to prove that phosphorescence is visible on the single-particle level. Highly diluted samples were prepared on microscopy glasses, which were placed on the microscope stage. A closed sample box on top of the table allows measuring under nitrogen conditions. Several different regions on the sample have been found, containing some agglomerated particles, but also isolated individual ones. Figure 3 shows that single particles are nicely identifiable.

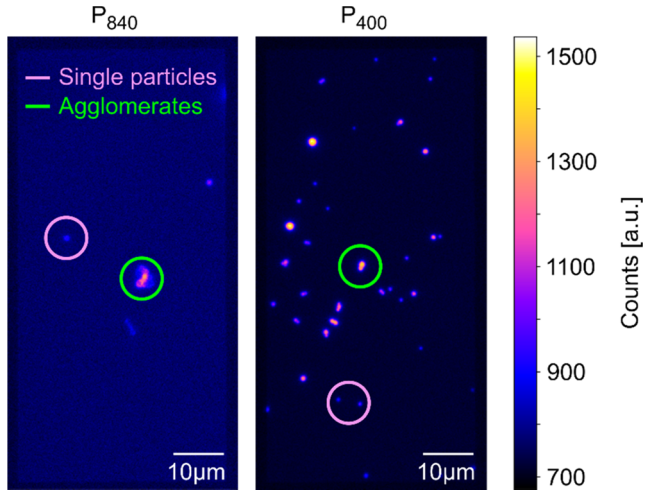

Figure 3. Images of the particles as visible in the microscope. It can be seen that both agglomerated particles and single particles are present in the film.

Interestingly, the optical properties between single particles and agglomerates do not differ strongly, which is a hint that agglomeration effects do not play a major role in our samples. The recorded image is spectrally divided into two channels: the first (Channel 1) is the wavelength regime of the fluorescence (below 450 nm) and the second (Channel 2) contains both the residual fluorescence and the phosphorescence (above 550 nm). The time behavior of a particle's emission can be determined using a series of pictures, where the cycle time, which is needed for one picture, determines the time resolution. The particle of interest is chosen in both the left and the right channel and the intensity of this spot is evaluated for the whole series of pictures. To isolate the phosphorescent contribution in Channel 2, the residual fluorescence needs to be quantified. Under ambient conditions (e.g., at the initial

https://doi.org/10.1021/acsomega.1c00785
ACS Omega 2021, 6, 13087−13093

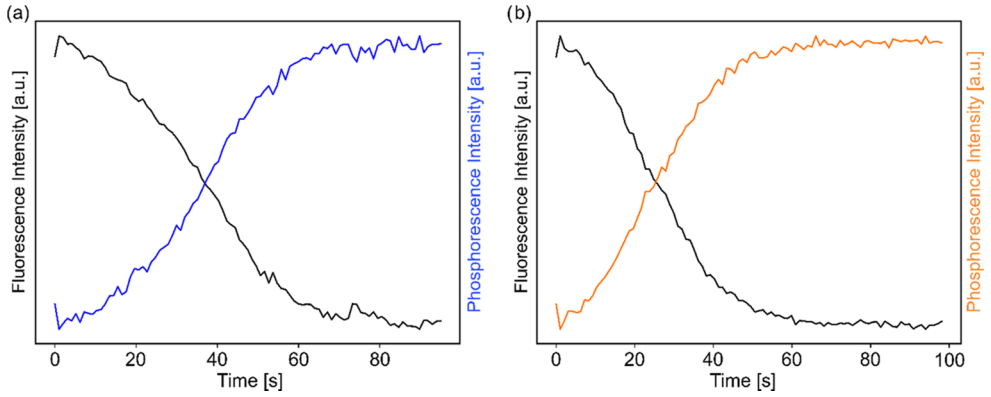

Figure 4. Right after having started the measurement, the nitrogen supply was opened to create an inert atmosphere (a) P_{840} and (b) P_{400}. Consequently, the phosphorescence increases, while the fluorescence decreases. Each measurement point is averaged over 10 images with an exposure time of ∼0.1 s, showing the behavior of one exemplary particle each.

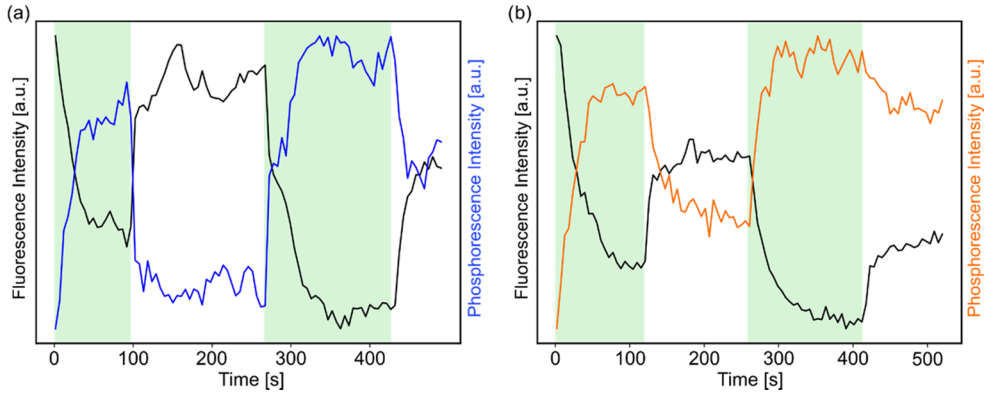

Figure 5. Appearance of phosphorescent emission of (a) P_{840} and (b) P_{400} is reversible, as can be seen in the switching behavior. The green area shows the time slot where nitrogen was switched on. Degradation leads to the fact that the initial signal level is not restored. Each measurement point is averaged over 10 images with an exposure time of ∼0.1 s.

time $t = 0$), Channel 2 only contains fluorescent emission. Now, the signal of Channel 1 can be scaled to this intensity and subsequently subtracted for the whole series of pictures. The residual signal is the remaining phosphorescence (for more details, see Figure S7). If no phosphorescence was present, this procedure would result in a constant zero intensity in Channel 2. For the particles, a clear switch-on process of the phosphorescence is visible, as can be seen in Figure 4, where the nitrogen supply was switched on right after the start of the detection. Hence, the phosphorescence signal increases steadily. Additionally, the fluorescence decreases, which is due to singlet−triplet annihilation and a saturation effect.[44] The latter is based on the lifetime of the phosphorescence, which has been determined to be around 600 ms, whereas the fluorescent lifetime is in the nanosecond range. Therefore, on the timescale of excitation and fluorescence, molecules that have undergone ISC to the triplet state are no longer available for further excitation, resulting in a lowered fluorescence signal. The timescale of the phosphorescence increase is determined by the nitrogen flow, the gas tightness of the sample box, and the permeability of the matrix.

This process is reversible, which means as soon as the nitrogen supply is stopped and oxygen penetrates back into the sample, the signal in the phosphorescent channel drops and only starts to rise again as soon as nitrogen is applied again (cf. Figure 5). The variations in the heights of the phosphorescent plateaus are due to the consequent scaling using the fluorescent signal. During the measurement, the emitter molecules and possibly the embedding polymers are subject to photodegradation (cf. Figure S4), influencing the fluorescence-to-phosphorescence ratio and thus changing the absolute height of the plateaus. Possible reasons are the formation of new molecular species with additional luminescence contributions to the overall signal and the increase of exciton quenching channels as a result of chemical decomposition of the embedding material.

The advantage of this particle system is that compared to other particles used in, e.g., tumor recognition, the singlet oxygen that is produced during irradiation does not harm the environment but is scavenged by PMMA.[45] So, in contrast to particles that help to destroy malignant cells, our particles might be used in bodies without harm after coverage with an oxygen barrier. Besides, they do not contain any toxic or costly metal compounds. To prevent the surrounding from getting damaged by UV light, RTP materials that absorb in the visible range, like PhenDpa[38] or BF_2(HPhN) (ref 5), could be used.

CONCLUSIONS

To summarize, we produced PMMA particles containing an organic emitter showing bright room temperature phosphorescence using a simple preparation route based on methyl methacrylate and TCATPB. Depending on the usage of a linker, the particles have a diameter between 840 and 400 nm. Upon illumination with 365 nm UV light, they can be detected

https://doi.org/10.1021/acsomega.1c00785
ACS Omega 2021, 6, 13087−13093

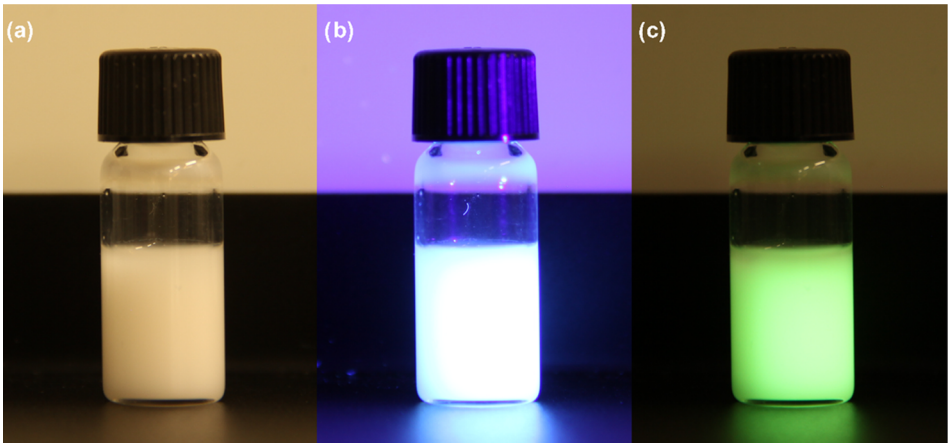

Figure 6. Photographs of a dispersion of P_{400} in water at (a) ambient light and (b, c) illumination with a 365 nm LED. (b) The prompt emission and (c) the delayed emission.

and visualized using a single-molecule spectroscopy setup. The fluorescent particles possess long-lived room temperature phosphorescence, which is activated in an inert nitrogen atmosphere or even in water in a sealed environment (see Figure 6) as soon as the oxygen is consumed. Exposure to the ambient atmosphere lets the phosphorescence disappear.

Overall, the switching between the two luminescence states is reversible. Since the PMMA matrix scavenges the singlet oxygen that is produced by illumination, these particles might be used in living bodies for in vivo imaging.

EXPERIMENTAL SECTION

Materials. TCATPB was synthesized from aniline and methyl-4-bromobenzoate by double Buchwald–Hartwig palladium coupling followed by oxidative coupling and saponification. A detailed procedure has been published recently.[35]

Methyl methacrylate (stabilized with hydroquinone monomethylether) was purchased from Sigma-Aldrich Chemical Co. and ethylene glycol dimethacrylate as well as sodium dodecyl sulfate from TCI chemicals. These chemicals were used without further purification.

Particle Preparation. P_{840}: 7.5 mg of $K_2S_2O_8$ in 2.5 mL of 1 μM SDS added to 2.5 μL of EGDMA, 247.5 μL of MAA, and 200 μL of 10 mg/mL TCATPB in cyclohexanol, and the reaction was stirred at 75 °C for 4 h.

P_{400}: 2.5 mg of $K_2S_2O_8$ in 2.5 mL of 1 μM SDS added to 250 μL of MAA and 200 μL of 10 mg/mL TCATPB in cyclohexanol, and the reaction was stirred at 75 °C for 4 h.

Sample Preparation. For the bilayer reference system, 164 μL of a 17 mM solution of TCATPB in anisole was added to a 1 mL solution of PMMA (80 mg/mL) also dissolved in anisole. Exceval (50 mg/mL) was dissolved in pure water at 120 °C in a closed vial. For spin coating, a speed of 2000 rpm and volumes of 150 μL (host and emitter) and 500 μL (pure barrier) were used to form a uniform film. The layers were coated on top of each other. Cleaned quartz glass substrates of a size of 25 mm × 25 mm were used. For P_{840} and P_{400} samples, 50 μL of the respective aqueous particle solution was added to 500 μL of a 50 mg/mL aqueous Exceval solution. The complete mixture was drop cast onto the substrate and dried at ambient conditions. For fluorescence/phosphorescence spectroscopy, P_{840} and P_{400} suspensions were diluted until optical clearness. Afterward, 500 μL of these solutions were drop cast onto quartz substrates and dried at ambient conditions.

Spectral Measurements. Direct and delayed emission measurements were performed using CAS 140CTS from Instrument Systems. To trigger the detection and the 300 nm (Thorlabs, M300L4) LED, a TGP3122 pulse generator (AIM-TTI Instruments) was used. The delayed spectra were recorded in the time span from a few to a few hundred milliseconds after turning off the LED. All measurements were performed in darkness under ambient conditions.

Lifetime Measurements. The phosphorescent lifetime was determined using a silicon photodetector PDA100A by Thorlabs. The decay was recorded and fitted using a two-exponential fit, yielding an intensity-averaged lifetime. The fluorescent lifetime was determined using time-correlated single-photon counting (TCSPC). The measurements were performed with an excitation laser PicoQuant LDHDC375, a PicoQuant PMA Hybrid-40 detector, a PicoQuant TimeHarp platine, and a monochromator SpectraPro HRS-300 from Princeton Instruments. To extract the lifetimes from the nanosecond decays, the reconvolution software FluoFit from PicoQuant was used.

Scanning Electron Microscopy (SEM). SEM characterization was performed with an Amray 1920 ECO SEM (SEMTech Solutions, Inc., Billerica, MA), operating at 10 keV, equipped with a scintillation detector (Everhart–Thornley). The particle suspensions were drop cast onto a sample holder equipped with a conductive sticker and left in air to dry for around one day. Afterward, the samples were sputtered with gold, using an Edwards S1508 sputter coater with an Ar pressure of 1.5×10^{-1} mbar for 60 s.

Fluorescence/Phosphorescence Microscopy. Fluorescence microscopy experiments were performed using a Nikon Ti2-A inverted microscope. The samples are placed on the microscope's table, which was applied with a custom-made box to allow measurements under inert conditions. The excitation light was from a 373 nm collimated free-beam laser diode (LDH-D-C-375, PicoQuant), passing a clean-up filter (370/36 BrightLine HC, Semrock) and a lambda fourth plate (355 nm, Edmund Optics). The beam was expanded using a 10× UV beam expander (BE10-UVB, Thorlabs, Inc.) and then focused on the back-focal plane of the objective to enable far-field microscopy. It entered the microscope through the backside port and was mirrored to the sample stage via a dichroic mirror

https://doi.org/10.1021/acsomega.1c00785
ACS Omega 2021, 6, 13087−13093

(zt 375 RDC, Chroma). Emitted light from the sample was collected by the objective and passed the dichroic mirror to be led to a side port of the microscope. Here, it was spectrally separated into two parts using color filters (FESH0450 and FELH0500, Thorlabs) and a dichroic mirror (zt 514 RDC, Chroma) mounted on an Optosplit II (Acal BFi Germany GmbH). The two resulting images represented the wavelength regimes. The image detection was done using a back-illuminated CCD camera (iXon Ultra 897, Andor). Time-resolved measurements were realized by taking a series of images and subsequent post-procession of the data with a self-written evaluation script.

■ ASSOCIATED CONTENT

Supporting Information

The Supporting Information is available free of charge at https://pubs.acs.org/doi/10.1021/acsomega.1c00785.

TCSPC spectra; XRD spectra; degradation experiments; oxygen sensitivity measurements; principle of particle imaging; phosphorescence activation experiment; and rate determination (PDF)

■ AUTHOR INFORMATION

Corresponding Author

Sebastian Reineke − *Technische Universität Dresden, Dresden Integrated Center for Applied Physics and Photonic Materials (IAPP), 01187 Dresden, Germany;* orcid.org/0000-0002-4112-6991; Email: sebastian.reineke@tu-dresden.de

Authors

Heidi Thomas − *Technische Universität Dresden, Dresden Integrated Center for Applied Physics and Photonic Materials (IAPP), 01187 Dresden, Germany*

Felix Fries − *Technische Universität Dresden, Dresden Integrated Center for Applied Physics and Photonic Materials (IAPP), 01187 Dresden, Germany*

Max Gmelch − *Technische Universität Dresden, Dresden Integrated Center for Applied Physics and Photonic Materials (IAPP), 01187 Dresden, Germany*

Toni Bärschneider − *Technische Universität Dresden, Dresden Integrated Center for Applied Physics and Photonic Materials (IAPP), 01187 Dresden, Germany*

Martin Kroll − *Technische Universität Dresden, Dresden Integrated Center for Applied Physics and Photonic Materials (IAPP), 01187 Dresden, Germany*

Thaleia Vavaleskou − *Johann Wolfgang Goethe-Universität Frankfurt am Main, Institut für Anorganische und Analytische Chemie, 60438 Frankfurt am Main, Germany*

Complete contact information is available at: https://pubs.acs.org/10.1021/acsomega.1c00785

Notes

The authors declare no competing financial interest.

■ ACKNOWLEDGMENTS

H.T., F.F., and M.G. did the experiments, prepared the manuscript, and received funding from the European Research Council (ERC) under the European Union's Horizon 2020 research and innovation program (grant agreement number 679213 "BILUM"). M.G. captured the photographs. T.B. performed the degradation experiment and the oxygen sensitivity measurement. M.K. conducted the XRD measurements and T.V. captured the SEM images.

■ REFERENCES

(1) Llano Suárez, P.; García-Cortés, M.; Fernández-Argüelles, M. T.; Ruiz Encinar, J.; Valledor, M.; Ferrero, F. J.; Campo, J. C.; Costa-Fernández, J. M. Functionalized phosphorescent nanoparticles in (bio)chemical sensing and imaging − A review. *Anal. Chim. Acta* **2019**, *1046*, 16−31.

(2) Zhang, C.; Zhang, K.; Zhao, T.; Liu, B.; Wang, Z.; Zhang, Z. Selective phosphorescence sensing of pesticide based on the inhibition of silver(I) quenched ZnS:Mn^{2+} quantum dots. *Sens. Actuators, B* **2017**, *252*, 1083−1088.

(3) Zou, W.-S.; Sheng, D.; Ge, X.; Qiao, J.-Q.; Lian, H.-Z. Room-Temperature Phosphorescence Chemosensor and Rayleigh Scattering Chemodosimeter Dual-Recognition Probe for 2,4,6-Trinitrotoluene Based on Manganese-Doped ZnS Quantum Dots. *Anal. Chem.* **2011**, *83*, 30−37.

(4) DeRosa, C. A.; Seaman, S. A.; Mathew, A. S.; Gorick, C. M.; Fan, Z.; Demas, J. N.; Peirce, S. M.; Fraser, C. L. Oxygen Sensing Difluoroboron β-Diketonate Polylactide Materials with Tunable Dynamic Ranges for Wound Imaging. *ACS Sens.* **2016**, *1*, 1366−1373.

(5) Lehner, P.; Staudinger, C.; Borisov, S. M.; Klimant, I. Ultra-sensitive optical oxygen sensors for characterization of nearly anoxic systems. *Nat. Commun.* **2015**, *5*, No. 4460.

(6) Kabe, R.; Notsuka, N.; Yoshida, K.; Adachi, C. Afterglow organic light-emitting diode. *Adv. Mater.* **2016**, *28*, 655−660.

(7) Kwon, W.; Do, S.; Lee, J.; Hwang, S.; Kim, J. K.; Rhee, S.-W. Freestanding luminescent films of nitrogen-rich carbon nanodots toward large-scale phosphor-based white-light-emitting devices. *Chem. Mater.* **2013**, *25*, 1893−1899.

(8) Braun, D.; Heeger, A. J. Visible light emission from semiconducting polymer diodes. *Appl. Phys. Lett.* **1991**, *58*, 1982−1984.

(9) Sun, W.; Yu, J.; Deng, R.; Rong, Y.; Fujimoto, B.; Wu, C.; Zhang, H.; Chiu, D. T. Semiconducting polymer dots doped with europium complexes showing ultranarrow emission and long luminescence lifetime for time-gated cellular imaging. *Angew. Chem. Int. Ed.* **2013**, *52*, 11294−11297.

(10) Dmitriev, R. I.; Borisov, S. M.; Düssmann, H.; Sun, S.; Müller, B. J.; Prehn, J.; Baklaushev, V. P.; Klimant, I.; Papkovsky, D. B. Versatile Conjugated Polymer Nanoparticles for High-Resolution O2 Imaging in Cells and 3D Tissue Models. *ACS Nano* **2015**, *9*, 5275−5288.

(11) Zhou, J.; Liu, Z.; Li, F. Upconversion nanophosphors for small-animal imaging. *Chem. Soc. Rev.* **2012**, *41*, 1323−1349.

(12) Ekins, R. P.; Dakubu, S. The development of high sensitivity pulsed light, time-resolved fluroimmunoassays. *Pure Appl. Chem.* **1985**, *57*, 473−482.

(13) Scorilas, A.; Diamandis, E. P. Polyvinylamine-streptavidin complexes labeled with a europium chelator: a universal detection reagent for solid-phase time resolved fluorometric applications. *Clin. Biochem.* **2000**, *33*, 345−350.

(14) Dmitriev, R. I.; Borisov, S. M.; Kondrashina, A. V.; Pakan, J. M. P.; Anilkumar, U.; Prehn, J. H. M.; Zhdanov, A. V.; McDermott, K. W.; Klimant, I.; Papkovsky, D. B. Imaging oxygen in neural cell and tissue models by means of anionic cell-permeable phosphorescent nanoparticles. *Cell. Mol. Life Sci.* **2015**, *72*, 367−381.

(15) Del Secco, B.; Ravotto, L.; Esipova, T. V.; Vinogradov, S. A.; Genovese, D.; Zaccheroni, N.; Rampazzo, E.; Prodi, L. Optimized synthesis of luminescent silica nanoparticles by a direct micelle-assisted method. *Photochem. Photobiol. Sci.* **2019**, *18*, 2142−2149.

(16) Vlakh, E. G.; Grachova, E. V.; Zhukovsky, D. D.; Hubina, A. V.; Mikhailova, A. S.; Shakirova, J. R.; Sharoyko, V. V.; Tunik, S. P.; Tennikova, T. B. Self-assemble nanoparticles based on polypeptides containing C-terminal luminescent Pt-cysteine complex. *Sci. Rep.* **2017**, *7*, No. 41991.

(17) Zangoli, M.; Pugliese, M.; Monti, F.; Bergamini, G.; D'Amone, S.; Ortolani, L.; Morandi, V.; Cortese, B.; Zanelli, A.; Gazzano, M.;

Maiorano, V.; Gigli, G.; Palamà, I. E.; Di Maria, F. Nanostructuring Iridium Complexes into Crystalline Phosphorescent Nanoparticles: Structural Characterization, Photophysics, and Biological Applications. *ACS Appl. Bio Mater.* **2019**, *2*, 4594−4603.
(18) Zhang, K. Y.; Zhang, J.; Liu, Y.; Liu, S.; Zhang, P.; Zhao, Q.; Tang, Y.; Huang, W. Core−shell structured phosphorescent nanoparticles for detection of exogenous and endogenous hypochlorite in live cells via ratiometric imaging and photoluminescence lifetime imaging microscopy. *Chem. Sci.* **2015**, *6*, 301−307.
(19) Miyashita, Y.; Horino, S.; Kasai, H.; Oikawa, H.; Nakanishi, H. Preparation and Luminescence Properties of Organic Phosphorescent Nanoparticles. *Jpn. J. Appl. Phys.* **2012**, *5*, No. 025002.
(20) Paramonov, D. V.; Kostryukova, T. S.; Bychenkova, T. A.; Pomelova, V. G.; Osin, N. S. Biospecific Nanoparticles for Multiplex Phosphorescence Analysis (PHOSPHAN). *Russ. J. Bioorg. Chem.* **2016**, *42*, 655−663.
(21) Marpu, S.; Upadhyay, P. K.; Nguyen, D. T.; Oswald, I. W. H.; Arvapally, R. K.; Petros, R. A.; Hu, Z.; Omary, M. A. Self-Assembly of Linear Polymers into Phosphorescent Nanoparticles: Optimization Toward Non-Cytotoxic Bioimaging and Photonic Devices. *J. Phys. Chem. C* **2015**, *119*, 12551−12561.
(22) Lloyd, D.; Williams, C. F.; Vijayalakshmi, K.; Kombrabail, M.; White, N.; Hayes, A. J.; Aon, M. A.; Krishnamoorthy, G. Intracellular oxygen: Similar results from two methods of measurement using phosphorescent nanoparticles. *J. Innovative Opt. Health Sci.* **2014**, *7*, No. 1350041.
(23) McClure, D. S. Triplet-Singlet Transitions in Organic Molecules. Lifetime Measurements of the Triplet State. *J. Chem. Phys.* **1949**, *17*, 905−913.
(24) Solovev, K. N.; Borisevich, E. A. Intramolecular heavy-atom effect in the photophysics of organic molecules. *Phys.-Usp.* **2005**, *48*, 231−253.
(25) Zhen, X.; Tao, Y.; An, Z.; Chen, P.; Xu, C.; Chen, R.; Huang, W.; Pu, K. Ultralong phosphorescence of water-soluble organic nanoparticles for in vivo afterglow imaging. *Adv. Mater.* **2017**, *29*, No. 1606665.
(26) Wang, X.-F.; Xiao, H.; Chen, P.-Z.; Yang, Q.-Z.; Chen, B.; Tung, C.-H.; Chen, Y.-Z.; Wu, L.-Z. Pure organic room temperature phosphorescence from excited dimers in self-assembled nanoparticles under visible and near-infrared irradiation in water. *J. Am. Chem. Soc.* **2019**, *141*, 5045−5050.
(27) Shi, H.; Song, L.; Ma, H.; Sun, C.; Huang, K.; Lv, A.; Ye, W.; Wang, H.; Cai, S.; Yao, W.; Zhang, Y.; Zheng, R.; An, Z.; Huang, W. Highly efficient ultralong organic phosphorescence through intramolecular-space heavy-atom effect. *J. Phys. Chem. Lett.* **2019**, *10*, 595−600.
(28) Cai, S.; Shi, H.; Li, J.; Gu, L.; Ni, Y.; Cheng, Z.; Wang, S.; Xiong, W.-w.; Li, L.; An, Z.; Huang, W. Visible-light-excited ultralong organic phosphorescence by manipulating intermolecular interactions. *Adv. Mater.* **2017**, *29*, No. 1701244.
(29) Li, Q.; Zhou, M.; Yang, Q.; Wu, Q.; Shi, J.; Gong, A.; Yang, M. Efficient room-temperature phosphorescence from nitrogen-doped carbon dots in composite matrices. *Chem. Mater.* **2016**, *28*, 8221−8227.
(30) Villa, M.; Del Secco, B.; Ravotto, L.; Roy, M.; Rampazzo, E.; Zaccheroni, N.; Prodi, L.; Gingras, M.; Vinogradov, S. A.; Ceroni, P. Bright Phosphorescence of All-Organic Chromophores Confined within Water-Soluble Silica Nanoparticles. *J. Phys. Chem. C* **2019**, *123*, 29884−29890.
(31) Wang, S.; Xu, M.; Huang, K.; Zhi, J.; Sun, C.; Wang, K.; Zhou, Q.; Gao, L.; Jia, Q.; Shi, H.; An, Z.; Li, P.; Huang, W. Biocompatible metal-free organic phosphorescent nanoparticles for efficiently multidrug-resistant bacteria eradication. *Sci. China Mater.* **2020**, *63*, 316−324.
(32) Ma, X.; Xu, C.; Wang, J.; Tian, H. Amorphous Pure Organic Polymers for Heavy-Atom-Free Efficient Room-Temperature Phosphorescence Emission. *Angew. Chem. Int. Ed.* **2018**, *57*, 10854−10858.
(33) Hirata, S.; Totani, K.; Zhang, J.; Yamashita, T.; Kaji, H.; Marder, S. R.; Watanabe, T.; Adachi, C. Efficient persistent room temperature phosphorescence in organic amorphous materials under ambient conditions. *Adv. Funct. Mater.* **2013**, *23*, 3386−3397.
(34) Kwon, M. S.; Lee, D.; Seo, S.; Jung, J.; Kim, J. Tailoring intermolecular interactions for efficient room-temperature phosphorescence from purely organic materials in amorphous polymer matrices. *Angew. Chem. Int. Ed.* **2014**, *53*, 11177−11181.
(35) Louis, M.; Thomas, H.; Gmelch, M.; Fries, F.; Haft, A.; Lindenthal, J.; Reineke, S. Biluminescence Under Ambient Conditions: Water-Soluble Organic Emitter in High-Oxygen-Barrier Polymer. *Adv. Opt. Mater.* **2020**, *8*, No. 2000427.
(36) El-hoshoudy, A. N. M. B. Emulsion Polymerization Mechanism. *Recent Res. Polym.* **2018**, DOI: 10.5772/intechopen.72143.
(37) Gmelch, M.; Thomas, H.; Fries, F.; Reineke, S. Programmable transparent organic luminescent tags. *Sci. Adv.* **2019**, *5*, No. eaau7310.
(38) Louis, M.; Thomas, H.; Gmelch, M.; Haft, A.; Fries, F.; Reineke, S. Blue-Light-Absorbing Thin Films Showing Ultralong Room-Temperature Phosphorescence. *Adv. Mater.* **2019**, *31*, No. 1807887.
(39) Su, Y.; Phua, S. Z. F.; Li, Y.; Zhou, X.; Jana, D.; Liu, G.; Lim, W. Q.; Ong, W. K.; Yang, C.; Zhao, Y. Ultralong room temperature phosphorescence from amorphous organic materials toward confidential information encryption and decryption. *Sci. Adv.* **2018**, *4*, No. eaas9732.
(40) Thomas, H.; Pastoetter, D. L.; Gmelch, M.; Achenbach, T.; Schlögl, A.; Louis, M.; Feng, X.; Reineke, S. Aromatic Phosphonates: A novel group of emitters showing blue ultra-long room temperature phosphorescence. *Adv. Mater.* **2020**, *32*, No. 2000880.
(41) Hirata, S. Recent Advances in Materials with Room-Temperature Phosphorescence: Photophysics for Triplet Exciton Stabilization. *Adv. Opt. Mater.* **2017**, *5*, No. 1700116.
(42) Hou, Y.; Jiang, G.; Gong, J.; Sha, R.; Wang, J. Recent Advances of Pure Organic Room Temperature Phosphorescence Materials for Bioimaging Applications. *Chem. Res. Chin. Univ.* **2021**, *37*, 73−82.
(43) Zhang, T.; Ma, X.; Wu, H.; Zhu, L.; Zhao, Y.; Tian, H. Molecular Engineering for Metal-Free Amorphous Materials with Room-Temperature Phosphorescence. *Angew. Chem., Int. Ed.* **2020**, *59*, 11206−11216.
(44) Salas Redondo, C.; Kleine, P.; Roszeitis, K.; Achenbach, T.; Kroll, M.; Thomschke, M.; Reineke, S. Interplay of Fluorescence and Phosphorescence in Organic Biluminescent Emitters. *J. Phys. Chem. C* **2017**, *121*, 14946−14953.
(45) Schiller, M.; Maier, R.-D. *Handbuch Kunststoff-Additive*; Hanser: München, 2016.

https://doi.org/10.1021/acsomega.1c00785
ACS Omega 2021, 6, 13087−13093